The Meteoritical Society

Meteoritics & Planetary Science 46, Nr 8, 1133–1151 (2011)
doi: 10.1111/j.1945-5100.2011.01219.x

MIL 03443, a dunite from asteroid 4 Vesta: Evidence for its classification and cumulate origin

Andrew W. BECK[1*], David W. MITTLEFEHLDT[2], Harry Y. McSWEEN Jr.[1], Douglas RUMBLE III[3], Cin-Ty A. LEE[4], and Robert J. BODNAR[5]

[1]Department of Earth and Planetary Sciences and Planetary Geoscience Institute, University of Tennessee, Knoxville, Tennessee 37996–1410, USA
[2]Astromaterials Research Office, NASA Johnson Space Center, Houston, Texas 77058, USA
[3]Geophysical Laboratory, Carnegie Institution of Washington, Washington, District of Columbia 20015, USA
[4]Department of Earth Science, Rice University, Houston, Texas 77005, USA
[5]Department of Geosciences, Virginia Tech, Blacksburg, Virginia 24061, USA
[*]Corresponding author. E-mail: abeck3@utk.edu

(Received 21 October 2010; revision accepted 06 May 2011)

Abstract–The absence of dunite (>90 vol% olivine) in the howardite, eucrite, and diogenite (HED) meteorite suite, when viewed with respect to spectroscopic and petrologic evidence for olivine on Vesta, is problematic. Herein, we present petrologic, geochemical, and isotopic evidence confirming that Miller Range (MIL) 03443, containing 91 vol% olivine, should be classified with the HED clan rather than with mesosiderites. Similarities in olivine and pyroxene FeO/MnO ratios, mineral compositions, and unusual mineral inclusions between MIL 03443 and the diogenites support their formation on a common parent body. This hypothesis is bolstered by oxygen isotopic and bulk geochemical data. Beyond evidence for its reclassification, we present observations and interpretations that MIL 03443 is probably a crustal cumulate rock like the diogenites, rather than a sample of the Vestan mantle.

INTRODUCTION

Differentiated bodies with chondritic starting compositions should contain olivine-rich lithologies such as peridotite (Ol + Opx + Cpx), harzburgite (Ol + Opx), and/or dunite (>90 vol% Ol) (Herzberg and O'Hara 1985). Melting models for asteroid 4 Vesta, the largest differentiated rocky body in the asteroid belt, suggest that it should contain dunite in its mantle or in crustal cumulates (Righter and Drake 1997; Ruzicka et al. 1997; Takeda 1997). Visible/near-infrared spectra of Vesta collected by ground-based telescopes and the Hubble Space Telescope (HST), interpreted to show regions containing significant olivine in the eastern hemisphere (Binzel et al. 1997; Gaffey 1997), support this hypothesis. The discovery of a large impact basin (460 km wide) at the southern pole of Vesta, which contains either an olivine-rich or high-calcium pyroxene-rich lithology (Thomas et al. 1997), may add further support for olivine-bearing ultramafic rocks on Vesta. This deeply excavated crater (13 km depth) would provide a geologically reasonable location for a Vestan dunite (Takeda 1997). However, other ground-based and HST investigations do not support the presence of extensive regions dominated by olivine-rich lithologies in the eastern hemisphere, or in ejecta material from the southern crater (Li et al. 2010 and Reddy et al. 2010; respectively). Nevertheless, modeling of HST images taken at four different band-passes suggests that olivine is a minor component intermixed with basaltic and orthopyroxenitic material, especially in the Western hemisphere (Shestopalov et al. 2010). Excavation of olivine-rich plutons smaller than the resolution of the HST imaging would be plausible sources for the olivine debris in the Western hemisphere.

Given the geochemical models suggesting olivine-rich rocks on Vesta, and the possibility of olivine-rich regions exposed by impacts, it would seem likely that dunites might be present among HED (howardite, eucrite, diogenite) meteorites, commonly thought to be samples from Vesta. However, HEDs containing up to only 60 vol% olivine have been reported (Bowman et al.

1997). These harzburgite diogenites make up a very small fraction (< 1%) of the entire HED 11 and 17 suite and show large intra-sample variation in olivine abundance (Bowman et al. 1997; Beck and McSween 2010a; Shearer et al. 2010). A few heterogeneous harzburgites such as these cannot account for the abundance of olivine predicted by differentiation models. Furthermore, identifying a dunite in the HED suite would provide support for spectroscopic interpretations of olivine-rich lithologies on the surface of Vesta.

Bunch et al. (2006) have suggested that Northwest Africa (NWA) 2968 may be a dunite sample related to the HED suite because the FeO/MnO ratios of its olivine and orthopyroxene are similar to those of olivine-bearing diogenites, and because its oxygen isotopic composition is similar to HEDs. However, the mg#s (molar Mg/(Mg + Fe) × 100) of olivine (92.5) and orthopyroxene (93) are slightly higher than the ranges typically observed for howardites or diogenites (see McSween et al. 2011), though some more magnesian olivines have been observed in other HED samples (Fuhrman and Papike 1981). NWA 5784 and NWA 5968 are also dunites that have been suggested to be related to the HED clan, but little information is available on them (Bunch et al. 2010).

The anomalous brecciated dunite Miller Range (MIL) 03443 (hereafter "MIL") is an olivine-rich achondrite. MIL was originally classified as a mesosiderite (McBride and McCoy 2006), based on its similarity to olivine-rich lithic clasts that have been reported in that group (e.g., McCall and Cleverly 1965; Ntaflos et al. 1993). However, during classification, it was noted that MIL displayed some characteristics that were similar to the HEDs. Preliminary reports have favored the reclassification of MIL as an HEDs with genetic relationships to diogenites (Krawczynski et al. 2008; Mittlefehldt 2008; Beck and McSween 2010b). Herein, we present a full petrographic description and detailed geochemical analysis of the meteorite using several different sections and splits from MIL 03443.

Given the high olivine abundance of MIL, it seems plausible that it would share the most commonalities with the other ultramafic member of the HEDs, the diogenites. We examine similarities between MIL and the diogenites using petrographic analyses of thin sections, bulk-rock chemistry, and oxygen isotope data. We also assess its petrogenesis in the context of magmatism on Vesta.

METHODS

Three thin sections of MIL were analyzed: 10, 11 (allocated to DWM), and 17 (allocated to HYM). Sections 10 and 11 were made from separate chips. Sections 11 and 17 were prepared from the same potted butt; three other sections were made from this same potted butt, between 11 and 17. Chemical analyses of section 17 were conducted at the University of Tennessee (UT), and sections 10 and 11 were analyzed at Johnson Space Center (JSC), both using Cameca SX-100 electron microprobes (EMP). Analytical conditions for sections 10 and 11 are as described by Mittlefehldt (1994), and those for section 17 are as described by Beck and McSween (2010a). Much of the diogenite data presented here for comparison is taken from referenced literature. However, for FeO/MnO ratios of diogenite orthopyroxene and olivine, we combine literature data with our own mineral analyses of 12 olivine-bearing diogenites, described by Beck and McSween (2010a).

A backscatter electron (BSE) image map of section 17 was used to calculate the modal mineralogy. Each mineral on the BSE map was assigned a specific grayscale threshold, and its relative abundance was calculated using ImageJ (Abramoff et al. 2004).

Mineral trace element compositions in MIL were acquired using an Agilent 7500ce inductively coupled plasma mass spectrometer (ICP-MS) combined with an Excimer 193 nm GeoLasPro Laser Ablation system (LA) at the Virginia Tech. The He gas flow was approximately 0.8 mL min^{-1} through an ablation cell with a volume of approximately 1.5 cm^3. Spot size ranged from 24 to 44 μm and dwell times ranged from approximately 15 to 30 s. NIST 610/612 glass was used as an external standard and analyzed four times before and after analysis. Previous workers have shown that abundances of most elements in silicate phases can be determined with better than 10% accuracy using the NIST 610/612 standards combined with a 193 nm excimer laser (Guillong et al. 2003; Sylvester 2008). Summation of major elements to 100% was used as an internal standard. Data reduction was achieved using the Analysis Management System software (Mutchler et al. 2008).

For bulk-rock geochemical analysis, an approximately 500 mg split was ground in a corundum mortar and pestle. The powder was quartered and mixed until an approximately 80 mg split was achieved. Similar sized powders of the United States Geological Survey (USGS) standards BCR2, PCC-1, and DTS-1 were also prepared. The sample and standard powders were then put into Savillex® beakers, and washed with 0.25 mL of concentrated HF and $HClO_4$ acids three times. The contents of the beakers were added to 125 mL polypropylene bottles and diluted with 2 wt% HNO_3 solution. A precisely weighed quantity of In solution was then added to each bottle, such that the concentration of In would be approximately 1 ppb. The solutions were then introduced into a ThermoFinnigan Element 2 magnetic sector ICP-MS using a small-volume cyclonic

spray chamber with an Elemental Scientific Teflon nebulizer, and with a free aspiration uptake rate of approximately 100 μL min^{-1}. A Pt guard electrode and a high sensitivity Ni skimmer cone were used. Relevant parameters were 13.43 L min^{-1} of Ar cool gas, 0.94 L min^{-1} of Ar sample gas, and 0.97 L min^{-1} of Ar carrier ("auxiliary") gas. Forward power was 1370 W, and reflected power was 2 W. Major elements were analyzed using a mass resolution ($m/\Delta m$) of approximately 3000 and trace elements at a resolution of approximately 300, which was sufficient to resolve all isobaric interferences (argides, oxides, and double-charged ions) relevant to the masses of interest in medium mass resolution (^{23}Na ^{27}Al, ^{39}K, ^{44}Ca, ^{45}Sc, ^{49}Ti, ^{51}V, ^{52}Cr, ^{53}Cr, ^{55}Mn, ^{56}Fe, ^{57}Fe, ^{59}Co, ^{60}Ni, ^{65}Cu, ^{66}Zn, ^{68}Zn). The USGS standards listed above were used for external calibration (standard values from Eggins et al. [1997] were used), and the 1 ppb In spike was used to compensate for instrumental drift. Procedural blanks were treated the same as samples and standards, and after correcting for instrumental drift, the blank intensities were subtracted from all samples and standards prior to external calibration. Uncertainties for measurements are < 5%.

Another crushed aliquot of MIL, weighing approximately 300 mg, was processed for oxygen isotope analysis. The entire aliquot was ultrasonicated for 5 min in dilute HCl, washed three times in deionized distilled water, and dried. Visual inspection of the acid-washed sample revealed submillimeter grains of a blue opaque phase, with thin brown filaments attached, that was interpreted to be a contaminant. The contaminant was removed by hand-picking under a 25X binocular microscope. Duplicate aliquots of the remaining sample weighing approximately 2 mg were loaded for oxygen isotope analysis. The resulting analyses, however, showed a higher dispersion in oxygen isotope ratios than is normally obtained for a homogeneous sample. Further characterization showed an additional contaminant, eventually identified as scraps of plastic, scraped from a threaded cap that had been forced onto the top of an unthreaded storage vial. After removal of contaminants by additional hand-picking, the remaining sample was reanalyzed for oxygen isotopes.

The repeatedly hand-picked, duplicate aliquots of MIL weighing approximately 2 mg were loaded into a reaction chamber for isotopic analysis (Sharp 1990). The loaded reaction chamber was heated and evacuated for several hours, repeatedly fluorinated with 25 torr of BrF_5 and evacuated, and then fluorinated overnight. Evacuation and fluorination were repeated the next morning until measured room-temperature fluorination products noncondensable in liquid nitrogen were reduced to a negligible blank. Analyses of individual samples were made by loading 25–30 torr of BrF_5 into the reaction chamber and heating the sample with a Synrad CO_2 infrared laser (30 w, 10.6 μm wavelength). The laser beam was defocused to a spot size of 100 μm diameter to minimize scattering of sample particles. The resulting mixture of O_2, SiF_4, and residual interhalogen compounds was purified by passage through two liquid nitrogen traps, and pumped by a single-stage Hg diffusion pump onto molecular sieve 5A chilled by liquid nitrogen. The purified sample was transferred to the dual inlet of a Thermo-Fisher MAT 252 mass spectrometer, where the ion beams of $^{16}O^{16}O$, $^{16}O^{17}O$, and $^{16}O^{18}O$ were measured (Rumble and Hoering 1994). Every sample was tested for NF_3 and CF_4 contamination by scanning the mass range from 40 to 75 Da with a Faraday cup whose preamplifier resistor had a value of 3×10^{11} Ω. Two aliquots of a reference material, Gore Mountain garnet (USNM 107144), were analyzed for every four unknowns. The reference garnet gives a value of $\delta^{18}O_{VSMOW}$ of 6.0 per mil in comparison to UWG-2 (Valley et al. 1995; Rumble et al. 1997). The 2σ standard deviations of Gore Mountain garnet analyses were as follows: $\Delta^{17}O \pm 0.03$, $\delta^{17}O \pm 0.09$; and $\delta^{18}O \pm 0.17$ per mil. The value used for the slope of the Terrestrial Fractionation Line (TFL) in this study is 0.526 (±0.001) (Rumble et al. 2007).

RESULTS

Petrographic Description and Mineral Abundances

MIL is a brecciated dunite dominated by 200–400 μm angular olivine grains set in a fine-grained, predominantly silicate, matrix. Olivine grains of up to 2.5 mm were observed (Fig. 1a). No "zoned phase sequence" coronas around olivine grains, which are common in mesosiderites (Nehru et al. 1980), were seen in any of the thin sections of MIL. Minor amounts of orthopyroxene, troilite, and chromite occur throughout the matrix. Fragmental orthopyroxene grains are subhedral and approximately 300 μm in size, whereas chromites are more euhedral and approximately 200 μm in size. Some grain fragments are composite grains containing olivine, orthopyroxene, and chromite preserving primary (nonbrecciated) contacts (Mittlefehldt 2008). The longest olivine-orthopyroxene contact is approximately 270 μm and the few preserved contacts do not give clear evidence whether they are igneous or metamorphic contacts. Troilite in the matrix occurs as large (approximately 800 μm) amoeboid blobs, possibly formed through impact melting. Metal is rare and only found as small blebs associated with troilite. Olivine grains contain small (50–75 μm) agglomerate inclusions that are euhedral, and composed of clinopyroxene ± troilite ± chromite ± metal. At low

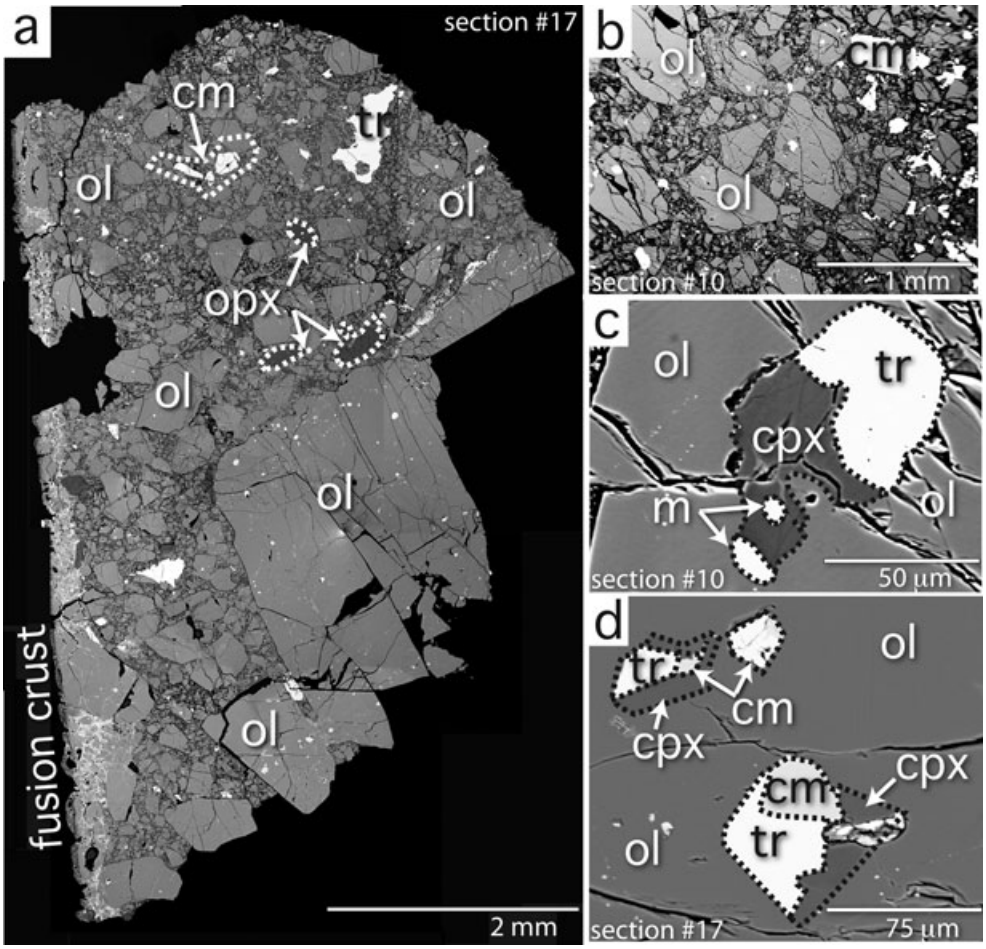

Fig. 1. a) Backscatter electron map of MIL 03443,17 showing its fragmental texture comprised mainly of olivine (ol) with smaller amounts of orthopyroxene (opx), chromite (cm), and troilite (tr). This composite image is 3340 × 2258 pixels. a,b) Larger olivine grains contain bright inclusions in backscatter that are composed of diopside (cpx), tr, ±cm, ±metal (m). c,d) Higher magnification images of these inclusions reveals relatively constant mineral proportions and negative-crystal shape.

magnification, these inclusions appear as bright areas scattered throughout larger olivine grains (Figs. 1a and 1b). At higher magnification, their euhedral, negative-crystal shapes and individual components are revealed (Figs. 1c and 1d). Well-developed fusion crust can be seen on one side of section 17 (Fig. 1a). Oxidation due to terrestrial weathering is present along most of the fusion crust.

The modal mineralogy of section 17 is: 91 vol% olivine, 5 vol% orthopyroxene, 1 vol% chromite, 0.7 vol% clinopyroxene, 2.3 vol% troilite, and < 1 vol% metal (Beck and McSween 2010a). Visual estimates of sections 10 and 11 give similar modes. Mineral abundances of another section of MIL (section 9) were estimated by Krawczynski et al. (2008) as > 90 vol% olivine, < 2 vol% orthopyroxene, and approximately 5 vol% chromite. Troilite was identified in section 9, but its abundance was not reported (Krawczynski et al. 2008). The similarity in modal abundances between these four sections suggests that mineral distributions are relatively homogeneous and that MIL can be best described as a fragmental monomict dunite breccia.

Mineral Compositions

Representative major, minor, and trace element concentrations for each mineral are given in Table 1. LA ICP-MS analyses were only conducted on section 17. Mineral major and minor element concentrations were not significantly different between the three thin sections studied; therefore, only one composition is listed for each mineral. Accordingly, in subsequent figures, results are not separated based on section number.

Table 1. Representative mineral compositions grouped by textural setting.

Textural setting	Large grains in the matrix					Small inclusions in olivine		
Mineral	Olivine	Opx.	Chromite	FeNi metal	Troilite	Cpx.	Chromite	Troilite
Microprobe analyses (wt%)								
SiO_2	38.2	55.0	0.09	b.d.	b.d.	54.2	0.08	b.d.
TiO_2	b.d.[a]	0.09	0.93			0.02	0.27	
Al_2O_3	b.d.	0.65	11.1			0.15	2.98	
Cr_2O_3	0.02	0.64	53.7			0.40	62.0	
V_2O_3	b.d.	b.d.	0.49			b.d.	0.90	
FeO_T	23.5	14.1	29.2			6.09	29.7	
MnO	0.55	0.51	0.64			0.29	0.70	
MgO	37.5	27.3	3.04			17.4	1.79	
CaO	0.12	1.40	b.d.			21.9	b.d.	
S				0.02	36.3			36.2
Fe				97.1	63.1			62.8
Ni	b.d.			0.95	0.03			b.d.
Co				0.94	b.d.			b.d.
P				b.d.	b.d.			b.d.
Total	99.9	99.7	99.2	99.0	99.4	100.5	98.5	99.0
Atomic formula								
Si	1.00	1.98	–			1.98	0.00	
Ti	–	0.00	0.02			0.00	0.01	
Al	–	0.03	0.46			0.01	0.13	
Cr	–	0.02	1.48			0.01	1.81	
V	–	–	0.01			–	0.03	
Fe	0.52	0.42	0.85			0.19	0.91	
Mn	0.01	0.02	0.02			0.01	0.02	
Mg	1.46	1.46	0.16			0.95	0.10	
Ca	0.00	0.05	–			0.86	–	
Total	3.00	3.99	3.00			4.01	3.01	
Wo	–	2.8	–			43.0	–	
En	–	75.4	–			47.6	–	
Fs	–	21.9	–			9.3	–	
Fe/Mn	42.3	27.1	–			20.6	–	
Fe#	26.0	22.5	–			16.4	–	
Laser ablation analyses (ppm)								
Sr	b.d.	0.36	b.d.					
Y	0.04	1.23	b.d.					
Zr	0.05	0.93	2.45					
Nb	b.d.	b.d.	0.23					
La	b.d.	0.03	b.d.					
Ce	b.d.	0.13	b.d.					
Nd	b.d.	0.18	b.d.					
Sm	b.d.	b.d.	b.d.					
Eu	b.d.	b.d.	b.d.					
Dy	b.d.	0.16	b.d.					
Er	b.d.	0.17	b.d.					
Yb	0.06	0.17	b.d.					

[a]Indicates analysis falls below detection limit.

Olivine and Pyroxene

Compositions of pyroxene and olivine in MIL fall near the magnesian end of known diogenite mineral compositions (Fig. 2). Some diogenites contain more Mg-rich orthopyroxene and olivine than MIL. Calcium concentrations in MIL olivine are on the high end of diogenite olivine compositions, which range from < 0.02 to 0.12 wt% CaO (Beck and McSween 2010a; Shearer et al. 2010). Other olivine minor and trace element abundances are quite low. Ni is below detection limits

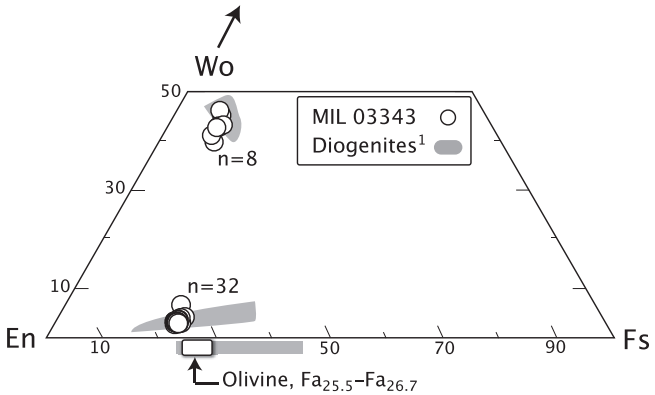

Fig. 2. Comparison of pyroxene and olivine compositions in MIL 03443 with those in diogenites. Olivine compositions are shown along the base. [1]Beck and McSween (2010a), Domanik et al. (2004), Fowler et al. (1994), Mittlefehldt (1994, 2000), Mittlefehldt and Lindstrom (1993), Shearer et al. (2010).

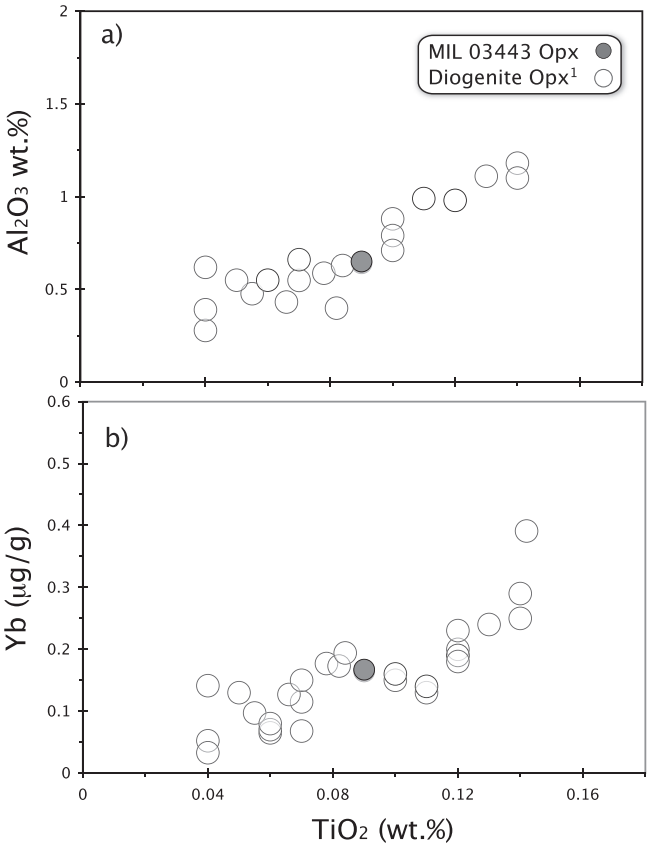

Fig. 3. Miller Range 03443 orthopyroxene (a) Al_2O_3 versus TiO_2 and (b) Yb versus TiO_2 concentrations compared with diogenite orthopyroxene. Similarities between orthopyroxene trace element concentrations between MIL 03443 and the diogenites suggest that they probably belong to the same meteorite group (HED), and that they had a similar origin (crustal cumulates). [1]Fowler et al. (1995), Mittlefehldt (1994).

for the EMP (< 0.02 wt%), and Cr_2O_3 is barely detectable at 0.02 wt%. Ni was not measured in olivine with LA ICP-MS. Abundances of Y and Zr in olivine were measured with LA ICP-MS, and their concentrations are 0.04 and 0.05 ppm, respectively. No Fe/Mg zoning was observed in MIL olivine, suggesting equilibration after crystallization. A high-current P X-ray map of one grain in section 17 was acquired. This high-current X-ray map revealed no P zoning in olivine (Balta and Beck 2011).

As described above, orthopyroxene (Ca-poor) occurs as larger grains in the matrix, whereas clinopyroxene (Ca-rich) forms small agglomerate inclusions within olivine. MIL orthopyroxene and clinopyroxene differ not only in textural setting, but also in their Fe#'s (Fe# = molar Fe/(Fe + Mg) × 100). Clinopyroxene inclusions are much more Mg-rich (low Fe#) than orthopyroxene (Table 1). MIL orthopyroxene has TiO_2 and Al_2O_3 concentrations that are generally in the middle of the range for diogenite orthopyroxene (see Fig. 3). The concentration of Cr_2O_3 in MIL orthopyroxene tends to be on the high end of the diogenite range (MIL = 0.64 wt% Cr_2O_3, diogenites 0.25–0.78 wt%, Beck and McSween 2010a; Fowler et al. 1994; Mittlefehldt 1994). As with the minor elements that are incompatible in orthopyroxene (Al_2O_3 and TiO_2), most incompatible trace elements in MIL orthopyroxene fall near the median of diogenite ranges as well (Fig. 3). The concentrations of the incompatible elements Y and Zr in MIL orthopyroxene (Y = 1.23 µg g^{-1}, Zr = 0.93 µg g^{-1}) are also in the mid ranges determined for diogenite orthopyroxenes (Y = 0.001–3.13 µg g^{-1}, Zr = 0.023–3.31 µg g^{-1}; Fowler et al. 1995).

Clinopyroxenes included in olivine were too small to acquire reliable LA ICP-MS data. Although clinopyroxene has been reported in some diogenites, it typically occurs as either exsolution lamellae in orthopyroxene (Mittlefehldt and Lindstrom 1993; Mittlefehldt 1994) or interstitially between orthopyroxene grains (Domanik et al. 2004), and has not been previously reported as inclusions in olivine (but see below).

The FeO/MnO wt% ratios in pyroxene and olivine can be used to identify a sample's parent body, and thus may be utilized in achondrite meteorite classification (Papike et al. 2003). Initial findings suggested that MIL olivine had ambiguous FeO/MnO values, falling between the mesosiderite and HED groups (McBride and McCoy 2006; Mittlefehldt 2008). Although compositions of some MIL olivine grains overlap both fields, the majority of the olivine FeO/MnO values clearly match the diogenites (Fig. 4a). Orthopyroxenes overlap both fields to a greater degree, but again, the majority of grains match the diogenites (Fig. 4b). MIL clinopyroxene inclusions,

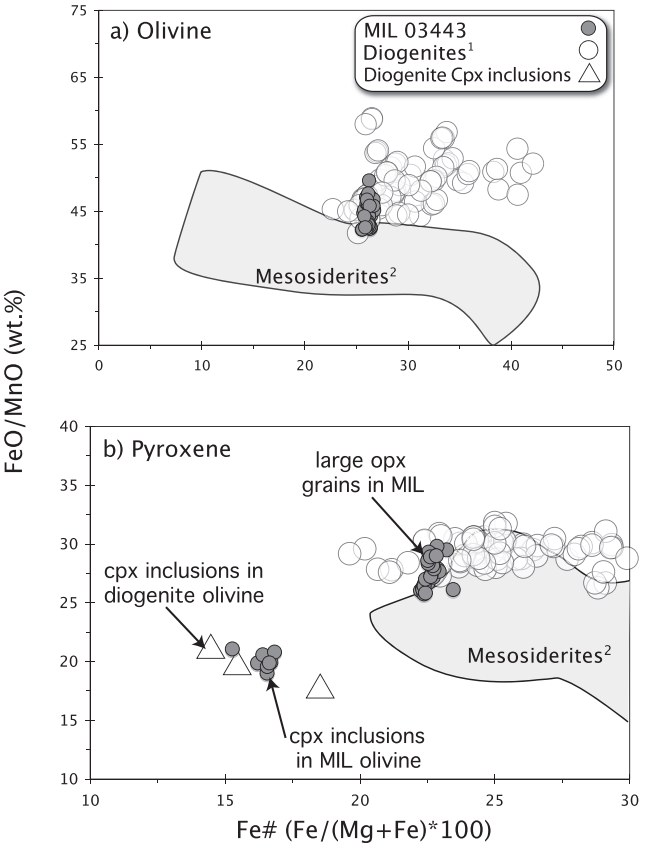

Fig. 4. FeO/MnO wt% ratios in MIL 03443 (a) olivine and (b) pyroxene compared with diogenites. Mesosiderite compositional ranges for these two minerals are enclosed by shaded area. Similarity in FeO/MnO ratios between MIL 03443 and diogenites suggests a common origin. [1]New data and McSween et al. 2011, including references therein; [2]Delaney et al. 1980; Kong et al. 2008; Mittlefehldt 1979, 1980; Mittlefehldt et al. 1998; Nehru et al. 1980; Prinz et al. 1980; Ruzicka et al. 1994; Wadhwa et al. 2003.

however, have FeO/MnO values that fall well below both the diogenite and mesosiderite pyroxene fields (Fig. 4b). This is probably due to the preferential distribution of $Ca > Mn^{2+} > Fe^{2+} > Mg$ into the pyroxene M2 site, leading to lower Fe and Mn in high-Ca pyroxenes relative to low-Ca pyroxenes (Papike 1981).

Our investigation has identified mineral inclusions in diogenite olivine that are texturally and compositionally very similar to those found in MIL olivine. We found these inclusions in three samples: Graves Nunataks (GRA) 98108, LaPaz Icefield (LAP) 03979, and Lewis Cliff (LEW) 88679. Pyroxene compositions in these diogenite olivine inclusions are plotted as triangles in Fig. 4b, where it can be seen that they match MIL in both FeO/MnO and Fe#. The pyroxenes in the diogenite inclusions have high-Ca contents, include agglomerates of chromite and/or troilite, are subhedral, and commonly

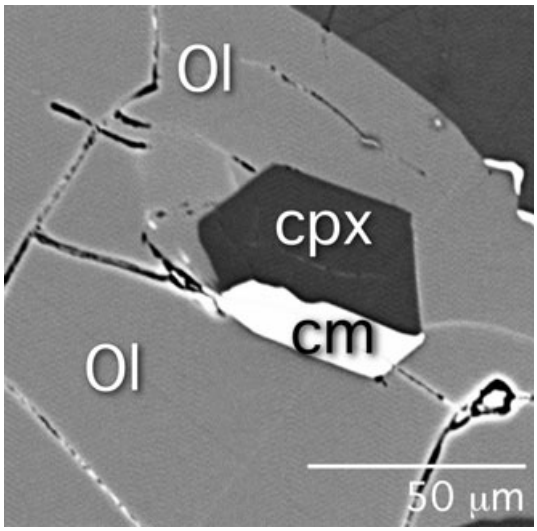

Fig. 5. A diopside (cpx) + chromite (cm) inclusion in olivine observed in diogenite LAP 03979. This inclusion is very similar in composition and texture to those in MIL 03443.

display negative-crystal forms (Fig. 5). All of these properties are also characteristic of the inclusions in MIL olivine. These clinopyroxenes included in diogenite olivine range in minor element concentration from 0.08 wt% TiO_2, 0.31 wt% Al_2O_3, and 0.12 wt% Cr_2O_3 in LEW 88679, to 0.30 wt% TiO_2, 1.50 wt% Al_2O_3, and 0.86 wt% Cr_2O_3 in LAP 03979. GRA 98108 clinopyroxene inclusions have compositions between these meteorites.

Chromite, Troilite, and FeNi Metal

Troilite in MIL does not show any significant compositional variation. Nor does FeNi metal, ranging from 0.67 to 0.95 wt% Ni and 0.94–2.15 wt% Co. Chromites, however, show variations in chemistry that are linked to textural setting (Fig. 6). Large, euhedral chromites in the matrix tend to be Al-rich with Cr#s (Cr# = Cr/(Cr + Al) × 100) ranging from 76 to 81. These chromites are similar in composition and texture to those found in diogenites (Bowman et al. 1999). We note that this range also overlaps chromites in mesosiderites (Powell 1971). Although indices similar to FeO/MnO in silicates have been developed to identify meteorite groupings for spinel (Papike et al. 2004), there are insufficient data at this time to chemically distinguish HED chromites from those in mesosiderites. The second chromite composition in MIL occurs as inclusions in olivine. These spinels are much more Cr-rich (Cr# 94) and fall well outside the field of known diogenite compositions (Fig. 6). Such spinel inclusions in olivine may have crystallized early from diogenite melts (Bowman et al. 1999).

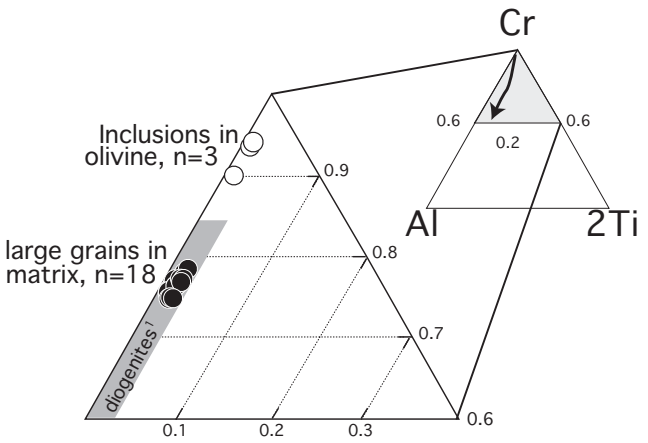

Fig. 6. Comparison of chromite compositions in MIL 03443 and diogenites. Black and white circles correspond to different textural settings. Gray area of plot at right indicates area of enlargement and also displays typical path of chromite chemical evolution. [1]Bowman et al. 1999.

Geochemistry

Bulk Geochemistry

The results of the ICP-MS analysis of MIL are presented in Table 2. Select elements are shown in element–element plots in Fig. 6, where they are compared with diogenite data obtained using ICP-MS analysis (Barrat et al. 1999, 2008, 2010a; Mittlefehldt et al. Forthcoming). MIL has a higher Cr content than typically found for diogenite whole-rock samples, (Fig. 7a) although Ellemeet, Garland, Meteorite Hills (MET) 00436, NWA 4215, and Shalka have comparable Cr contents (Barrat et al. 2006, 2008; Fredriksson et al. 1976; McCarthy et al. 1972; Mittlefehldt 1979, 1994; Mittlefehldt et al. Forthcoming). The high Cr content is most plausibly a reflection of a higher modal chromite content for MIL compared with that typical of diogenites (diogenites can contain up to 5 vol% chromite, but typically contain 0.5–1 vol% chromite, Bowman et al. 1997). Chromite is a major host for V in MIL (Table 1) and diogenites (Mittlefehldt 1994; Bowman et al. 1999). In spite of its higher chromite content, the V content of MIL is at the lower end of the range observed for diogenites. On the basis of in situ measurements of diogenites (Shearer et al. 2010), we expect that orthopyroxene in MIL has a much higher V content than does the olivine. The V_{opx}/V_{ol} ratios of the seven diogenites measured by Shearer et al. (2010) vary from 6.4 to 27.1. The low V content for MIL compared with many diogenites plausibly represents a lower V content of the silicate minerals because of the much higher modal olivine content. The contents of the incompatible lithophile elements Al, Ti, Sm, and Yb are lower in MIL than in diogenites, with a few exceptions (Figs. 7b and 7c). The moderately siderophile element Co is higher in MIL than found for any of the diogenites, whereas the Ni content is at the high end of the diogenite range (Fig. 7d).

Oxygen Isotopes

Oxygen isotopic composition is a proven method of classifying achondrite meteorites (Clayton and Mayeda 1996). Achondrite parent bodies became homogenized in oxygen isotopes (^{16}O, ^{17}O, and ^{18}O) during differentiation, and subsequent mass-dependant fractionation causes all samples from a particular body to fall upon a single oxygen isotope fractionation line (Clayton and Mayeda 1996). Herein, we compare MIL oxygen isotopic compositions to those of other HEDs. Our data are reported in $\delta^{18}O$ [$\delta^{18}O = (^{18}O/^{16}O)_{MIL}/(^{18}O/^{16}O)_{SMOW}$; where SMOW = standard mean ocean water] and $\Delta^{17}O$ [$\Delta^{17}O = (\delta^{17}O - 0.52*\delta^{18}O)$; where $\delta^{17}O$ is calculated similar to $\delta^{18}O$ above]. In our two analyses, we measured MIL to contain −0.197 and −0.236 $\Delta^{17}O$, and 3.04 and 3.14 $\delta^{18}O$. The oxygen isotopic composition of MIL matches with that of other HEDs. MIL has the same $\Delta^{17}O$ values as individual eucrite and diogenite analyses, and is within error of the well-defined mean $\Delta^{17}O$ for all HEDs (Fig. 8).

DISCUSSION

Classification

Although the oxygen isotopic composition of MIL matches the HEDs quite well, there is sufficient overlap between mesosiderite and HED oxygen isotope values to draw a classification solely based on this evidence in question (Fig. 8) (Greenwood et al. 2005, 2006). We turn to a comparison of mineral chemistries, specifically silicate FeO/MnO, to better determine if MIL is an HED or a mesosiderite lithic clast.

Compositions of minerals in MIL, specifically FeO/MnO in olivine and pyroxene, may be used to determine whether MIL should be classified as an HED or mesosiderite. As a result of their similar behavior in igneous systems, the ratios of FeO to MnO can be used to argue for common parent bodies for meteorites, and thus proper classification (Papike et al. 2003). Though it appears that MIL has undergone metamorphic equilibration, which will be discussed below, the original FeO/MnO ratio should not be affected. Equilibration may alter the total concentrations of FeO + MnO, but due to their similar behaviors in geochemical systems, it would preserve the original ratio.

Although there is overlap between the mesosiderite and HED FeO/MnO fields, it is not as complete as for $\Delta^{17}O$. We attempted to minimize this overlap as much as possible by comparing FeO/MnO in MIL only with the

Table 2. Bulk composition of MIL 03443,14 and control samples determined using ICP-MS.

			DTS-1		PCC-1				BCR-2
		MIL 03443,14	This work	G-94	This work	G-94	This work	USGS	GeoReM
Li	μg g^{-1}	0.48	1.91	**2.1**	1.18	1.6	8.95	*9*	*9*
Mg	mg g^{-1}	218	298	**299**	284	**261.9**	20.3	**21.6**	**21.6**
Al	mg g^{-1}	2.5	1.12	1	3.94	**3.57**	69.9	**71.4**	**71.4**
P	μg g^{-1}	13.4	7.8	9	11.8	9	1570	**1500**	**1530**
Ca	mg g^{-1}	1.87	0.922	**1.2**	4.07	**3.7**	47.5	**50.9**	**50.9**
Sc	μg g^{-1}	5.2	3.80	3.5	8.75	**8.4**	31.4	**33**	**33**
Ti	μg g^{-1}	171	25.0	30	33.4	60	13500	**13500**	**13500**
V	μg g^{-1}	104	12.5	11	34.8	**31**	404	**416**	**416**
Cr	mg g^{-1}	10.1	3.52	**3.99**	2.63	**2.73**	0.0272	**0.018**	**0.018**
Mn	mg g^{-1}	4.07	0.987	**0.93**	0.998	**0.93**	1.47	**1.52**	**1.52**
Fe	mg g^{-1}	197	61.5	**60.7**	60.8	**57.7**	87.3	–	**96.5**
Co	μg g^{-1}	49	140	**137**	118	**112**	36.4	**37**	**37**
Ni	μg g^{-1}	61	2400	**2360**	2450	**2380**	14.4	–	*18*
Cu	μg g^{-1}	10.1	8.00	7.1	7.85	10	24.4	*19*	*21*
Zn	μg g^{-1}	6.3	49.1	46	45.2	42	128	**127**	**127**
Ga	μg g^{-1}	0.99	0.552	*0.5*	0.813	*0.7*	22.3	**23**	**23**
Rb	ng g^{-1}	50	72	58	73.6	**66**	46100	**48000**	46900
Sr	μg g^{-1}	0.108	0.3	0.32	0.578	**0.4**	332	**346**	340
Y	μg g^{-1}	0.208	0.0399	0.04	0.0949	*0.1*	37.7	**37**	**37**
Zr	μg g^{-1}	0.46	0.209	*4*	0.216	10	192	**188**	184
Nb	ng g^{-1}	58	37.3	*2200*	19.8	*1000*	12400	–	12600
La	ng g^{-1}	6	25.7	29	36.9	52	25100	**25000**	24900
Ce	ng g^{-1}	13.9	48.2	72	64.6	100	53400	**53000**	52900
Pr	ng g^{-1}	1.7	5.9	**6.3**	7.9	13	6660	*6800*	6700
Nd	ng g^{-1}	9.2	22.7	29	29.4	42	28400	**28000**	28700
Sm	ng g^{-1}	5.2	5.3	4.6	5.2	6.6	6440	*6700*	6580
Eu	ng g^{-1}	1.1	1.4	1.2	2.4	1.8	2200	**2000**	1960
Gd	ng g^{-1}	10.4	4.3	*3.8*	7.2	*14*	6780	**6800**	6750
Tb	ng g^{-1}	2.3	0.7	0.8	1.3	1.5	1070	*1070*	1070
Dy	ng g^{-1}	20.3	5.0	*3*	9.7	10	6300	–	6410
Ho	ng g^{-1}	6.7	1.3	*1.3*	3	2.5	1270	*1330*	1280
Er	ng g^{-1}	29.1	4.9	*4*	12.4	*12*	3630	–	3660
Tm	ng g^{-1}	5.5	1.1	1.4	2.5	2.7	524	*540*	540
Yb	ng g^{-1}	45	9.4	10	23.6	24	3300	**3500**	3380
Lu	ng g^{-1}	9.3	2.0	2.4	4.8	5.7	486	*510*	503
Hf	ng g^{-1}	9.8	4.3	15	4.6	*40*	4590	*4800*	4900
Ta	ng g^{-1}	1.9	1.6	39	2.9	*20*	736	–	740
Th	ng g^{-1}	2.4	10	10	10.9	13	6010	**6200**	5700

For control samples, recommended or certified values in bold font, proposed values in regular font, and information-only values in italic font. References for literature values: G-94 = Govindaraju (1994); USGS = Certificate of Analysis (available on the USGS website: http://minerals.cr.usgs.gov/geo_chem_stand/basaltbcr2.html); GeoReM = preferred values from the Geological and Environmental Reference Materials website (http://georem.mpch-mainz.gwdg.de/).

diogenites. We did not use eucrites because they have been shown to have a modest range of FeO/MnO ratios (Mayne et al. 2009), and because diogenites have measurably different FeO/MnO ratios than the eucrites (Papike et al. 2001). Similarly, we excluded howardites, because they are regolith breccias and may contain chondritic and other foreign clasts (Mittlefehldt et al. 1998), which would have non-HED FeO/MnO. As shown in Fig. 4, FeO/MnO ratios in both MIL olivine and pyroxene match the diogenites much better than they match the mesosiderites. The majority of grains of both of these minerals plot with the diogenites above the mesosiderite field. This suggests that MIL belongs with the HEDs.

Petrographic evidence is more ambiguous. The lack of FeNi metal in MIL and the lack of olivine coronas, both ubiquitous in mesosiderites, would seem to suggest that MIL belongs with the HEDs, where these are absent. However, if MIL were a mesosiderite lithic clast, the paucity of FeNi metal and lack of olivine coronas

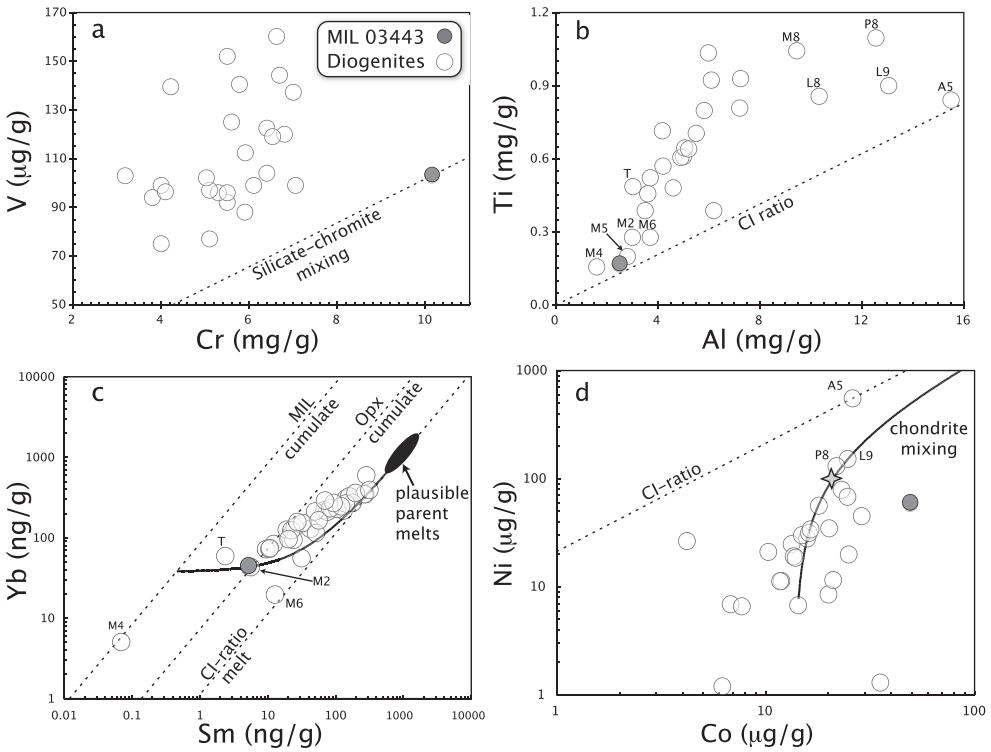

Fig. 7. Comparison of element–element diagrams for MIL 03443 and diogenites. In (a), the silicate-chromite mixing line is a tie-line between average chromite (Table 1) and an olivine-orthopyroxene mixture, as given by the modal mineralogy of MIL 03443, approximately 95:5. The Cr contents for olivine, orthopyroxene and chromite, and the V content of chromite, were taken from Table 1. Vanadium in the olivine-orthopyroxene mixture was assumed to be 15 μg g^{-1}. This is a plausible estimate based on the V contents of olivine and orthopyroxene in diogenites for the mixing ratios we have used (Shearer et al. 2010). In (b), labeled diogenites with >8 mg g^{-1} Al are all plagioclase-bearing. In (c), the CI-ratio melt line is a locus of fictive melts with CI Yb/Sm ratios. The cumulate opx line is the locus of orthopyroxenes that would be in equilibrium with such melts. The MIL cumulate line is the locus of cumulates with the olivine/orthopyroxene ratio of MIL 03443 that would be in equilibrium with such melts. The field labeled "plausible parent melts" is the area where melts parental to those diogenites that plot on the cumulate orthopyroxene line would lie. The curved line is a mixing line between a MIL cumulate and its equilibrium melt, constrained to pass through the MIL 03443 datum. The partition coefficients used to calculate these lines and field are given in the text. In (d), the curve is a mixing line between a low-Ni diogenite and a chondritic clast from the diogenite Ellemeet (Mittlefehldt 1994). The four-pointed star indicates a 1% contamination level. Labeled diogenites are polymict mixtures of diogenitic and eucritic material. The labeled diogenites are: A5—ALH 85015, L8—LEW 88008, L9—LAP 03979, M2—MET 00422, M4—MET 00424, M5—MET 00425, M6—MET 00436, M8—MET 01084, P8—PCA 02008, and T—Tatahouine. Sources of diogenite data are given in the text.

may be expected. Other mesosiderite ultramafic lithic clasts reported contain low amounts of metal (McCall and Cleverly 1965; Ntaflos et al. 1993), and due to the formation of coronas in mesosiderite olivine through a redox reaction with the metal-rich matrix (Ruzicka et al. 1994), olivine coronas would be expected to be absent in a mesosiderite lithic clast containing minerals that had no direct contact to the metal-rich matrix.

The small clinopyroxene ± troilite ± chromite ± metal inclusions in MIL olivine provide an additional link to the HEDs. Three diogenites (GRA 98108, LEW 88679, and LAP 03979) contain olivine with inclusions having very similar mineral compositions and textures to the inclusions in MIL, as discussed above. In a review of 10 mesosiderites, Powell (1971) described similar inclusions to those we have observed in MIL olivine. However, the inclusions described by Powell (1971) occur predominantly in pyroxene, not olivine, and are composed solely of opaque phases, not diopside + opaques. Olivine inclusions have been described in the Budulan mesosiderite; however, these inclusions appear symplectic, and are composed of opaques + orthopyxroxene, not opaques + diopside (Lorenz et al. 2010). Two possible explanations exist for the occurrence of identical olivine inclusions in both the diogenites and MIL: either (1) MIL and the diogenites formed by similar processes and from similar melts or (2) they have been intermixed through brecciation. Both of these explanations strongly suggest that the parent body of MIL is the same as that of the diogenites, i.e., asteroid 4 Vesta.

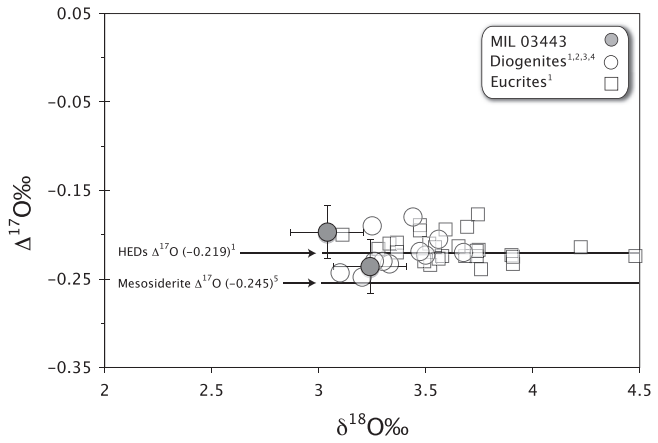

Fig. 8. Comparison of oxygen isotope compositions of MIL 03443 with the HEDs $\Delta^{17}O$ average and individual eucrite and diogenite analyses. [1]Wiechert et al. (2004), [2]Clayton and Mayeda (1996), [3]Barrat et al. (2006), [4]Bunch et al. (2010), [5]Greenwood et al. (2006).

The lack of preserved igneous zoning in MIL olivine also supports grouping it with the diogenites. It is widely thought that the diogenites have undergone substantial postcrystallization equilibration, which has erased any variability in major element concentrations from the cores to rims of pyroxene grains (Fowler et al. 1994; Mittlefehldt 1994). This same Fe/Mg equilibration is seen in diogenite olivine (Beck and McSween 2010a; Shearer et al. 2010). In MIL, the lack of preserved zoning of Fe/Mg in olivine generally supports a postcrystallization equilibration history as well. The ratio of orthopyroxene Fe# to olivine Fe# in MIL (0.86) matches that calculated for an equilibrium assemblage of low-Ca pyroxene and olivine crystallizing from eucritic melts (0.86, Stolper 1977), and matches orthopyroxene to olivine Fe# ratios in harzburgitic fragments of other diogenites (0.79–0.91), which were calculated to have equilibrated at approximately 1100 °C (Beck and McSween 2010a). The similarity in metamorphic history between MIL and the diogenites supports the conclusion that MIL is part of the diogenite group.

As was originally proposed in Beck and McSween (2010a), MIL should be called a "dunitic diogenite," rather than inventing a new named class of HED. The subgrouping of diogenites into dunitic, harzburgitic, and orthopyroxenitic follows the previous division of basaltic and cumulate eucrites (Delaney et al. 1984) and of basaltic, olivine-phyric, and lherzolitic shergottites (Goodrich 2002), where each subgroup shares a common petrologic origin. As will be shown in the next few sections, MIL shares a common petrologic origin with the diogenites and thus should be grouped with them.

NWA 2968 and Other Potential HEDs Dunites

As mentioned in the Introduction, Bunch et al. (2006) have suggested that NWA 2968 may be a dunite sample related to the HED suite. This meteorite contains olivine that is substantially more magnesian than olivine in MIL (NWA Mg# 92.5, MIL Mg# 74), but the FeO/MnO ratios are similar (NWA 48, MIL 42.3). Olivine in NWA 2968 is slightly higher in Mg# than the ranges typically observed for howardites or diogenites, which typically have olivine with Mg# < 92 (Delaney et al. 1980; Fuhrman and Papike 1981; Hewins 1981; Desnoyers 1982; Sack et al. 1991; Mittlefehldt 1994, 2000; Beck and McSween 2010a; Shearer et al. 2010). However, some more magnesian olivines have been observed. Desnoyers (1982) found two grains in howardites with Mg#s of 98.5 and 99. The former was in a chondritic clast in Bununu, whereas the latter was in the matrix of Kapoeta. Fuhrman and Papike (1981) reported one grain in Bholgati with an Mg# of 95.9. With the exception of one grain from a chondritic clast (Desnoyers 1982), the textural contexts for these magnesian olivines have not been described in sufficient detail to determine whether they are innate to the HED parent asteroid or exogenic.

Northwest Africa 2968 contains orthopyroxene that is again more magnesian than MIL (NWA Mg# approximately 93, MIL Mg# 77.5), but has similar FeO/MnO (NWA 26, MIL 27.1) (Bunch et al. 2006). The NWA 2968 orthopyroxene Mg# is also higher than known for diogenites or lithic clasts in howardites (max Mg# reported 86–84) (Fredriksson and Keil 1963; Labotka and Papike 1980; Fuhrman and Papike 1981; Mittlefehldt 2002; Barrat et al. 2008). Thus, orthopyroxene in NWA 2968 is substantially more magnesian than found for bona fide HED meteorites.

The silicate compositions in NWA 2968 are not good matches to those calculated in models for the crystallization of putative Vesta compositions. Ruzicka et al. (1997) calculate that the initial olivine to form in their fractional crystallization model for Vesta has an Mg# of 93, similar to that of NWA 2968 olivine. However, the most magnesian pyroxene in this model has an Mg# of only approximately 84, much lower than that of NWA 2968. Similarly, the Vestan magma ocean model of Righter and Drake (1997) would generate olivine with Mg# like those in NWA 2968, but orthopyroxene with Mg# lower than those found in that meteorite. Thus, the mineral compositions for NWA 2968 are not good matches for models that otherwise produce moderate to good simulations of HED mineralogy and composition.

Northwest Africa 2968 contains pyrrhotite with 1.7–4.7 wt% Ni, and troilite containing 0.36 wt% Ni (Bunch

et al. 2006). In contrast, the few troilite grains analyzed in HED's are very low in Ni, with approximately 0.01 wt% (Floran et al. 1981; Mittlefehldt 2000). Troilite in MIL contains 0.03 wt% Ni (Table 1). Pyrrhotite has not been reported in HEDs (Rubin 1997).

The oxygen isotopic composition of NWA 2968 (Bunch et al. 2006; Scott et al. 2009a) is within the ranges reported for HEDs and mesosiderites (Wiechert et al. 2004; Greenwood et al. 2005, 2006; Scott et al. 2009b), and thus is permissive of, but does not require, an HED's origin. Bulk samples of NWA 2968 have high Ni and Co contents (Barrat et al. 2008), which are not observed in diogenites (Mittlefehldt 1994, 2000; Barrat et al. 2008, 2010b) or MIL (Table 2). Barrat et al. (2010b) also report that NWA 2968 has an unusual La/Sm ratio of 5.5 times CI. Extreme light REE enrichments are known for bulk mesosiderite samples (Mittlefehldt et al. 1979), but have not been observed in bulk samples of HEDs (e.g., Mittlefehldt and Lindstrom 2003; Barrat et al. 2008, 2010a; Warren et al. 2009) or in MIL (this work).

Although it has been suggested that NWA 2968 is a dunite related to HEDs (Bunch et al. 2006), there are substantial mineralogical and compositional reasons to doubt a relationship between them. A detailed petrologic and compositional study of NWA 2968 is needed before kinship with the HED clan can be validated. Two other dunites have recently been discussed as possible HED relatives—NWA 5784 and NWA 5968—but only limited information is available (Bunch et al. 2010). To date, only MIL 03443 can be convincingly attributed to the HED parent asteroid.

Petrogenesis: Crustal Cumulate Versus Mantle Residuum Origin

Mineralogic Evidence

On Earth, dunites occur in a variety of geologic settings, and can be formed by different processes. They may represent solid residues from a high degree of partial melting, or cumulates formed using fractional crystallization of olivine. Both processes can produce, from bottom up, a dunite-harzburgite-orthopyroxenite stratigraphic sequence. An example of partial melting residuum is the basal dunite in an ophiolite sequence. These dunites contain olivine with higher Mg#s than any of the overlying units, which were either derived from the extruded basaltic magma or lesser degrees of partial melting (e.g., Pallister and Hopson 1981). By the same measure, residual dunites contain the most Cr-rich spinel, Mg-rich pyroxene, Cr-rich olivine, and are lacking in Ca- and Al-rich phases, relative to overlying lithologies (e.g., Pallister and Hopson 1981; Tamura and Arai 2006). In contrast, fractional crystallization may produce cumulate dunites that contain olivine and pyroxene with lower Mg#s, along with lower Cr# spinel, relative to the overlying harzburgites and orthopyroxenites (e.g., the cryptic layering of the Bushveld Complex [Eales and Cawthorn 1996] and the Stillwater Complex [Jackson 1961]). Herein, we consider the composition of MIL with respect to the two scenarios described above, and with respect to the diogenites, which are harzburgites and orthopyroxenites from Vesta. In a partial melting scenario, MIL would represent the residual mantle from which diogenitic melts were extracted. In the fractionation scenario, both MIL and the two types of diogenites would have formed as cumulates from fractionating magmas.

The silicates in MIL, although Mg-rich, are not the most magnesian in the HEDs suite. Some diogenites contain orthopyroxene and olivine that are more Mg-rich than those found in MIL (white circles with low Fe# in Figs. 4a and 4b). Bilanga, Elephant Moraine (EETA)79002, LAP 02216, Mangaon, MET 00425, PCA 02008, and Queen Alexandra Range (QUE) 99050 all contain orthopyroxene with Mg#s higher than those in MIL (Mg# 77.6–85 versus 77.5 in MIL; Barrat et al. 2008; Beck and McSween 2010a; Domanik et al. 2004; Mittlefehldt 1994, 2000); (Table 1). Similarly, diogenites EETA79002, LAP 02016, and PCA 02008 contain olivine with Mg#s higher than those in MIL (ol Mg# 74.1–85.5 versus 74 in MIL; Beck and McSween 2010a; Mittlefehldt 2000); (Table 1). MIL olivine also contains Cr concentrations similar to those in other diogenites (Beck and McSween 2010a; Shearer et al. 2010). Cr#s of larger spinels in MIL are well within the range of other diogenites (Bowman et al. 1999), as seen by the overlap between the MIL data and published diogenite compositions in Fig. 5. Finally, MIL orthopyroxene has incompatible minor and trace element concentrations that fall in the middle of the diogenite orthopyroxene range (Fig. 3). All of the above lines of evidence suggest that MIL is not a mantle restite (a residuum after partial melting), but rather a cumulate, and is probably part of a fractionation sequence that includes the diogenites. This relationship is bolstered by the presence of clinopyroxene ± troilite ± chromite ± metal inclusions in olivine from both MIL and the diogenites. These inclusions suggest that both MIL and the diogenites were formed from similar processes and from similar melts. Similarly, identical olivine to orthopyroxene Fe# ratios (0.86) of MIL and the diogenites suggests a common metamorphic history, and thus supports a common petrologic origin. We propose that MIL represents a cumulate dunite from a fractionating magma, which, as it evolved, then produced harzburgitic and orthopyroxenitic diogenites.

Bulk Chemistry Evidence

The lithophile trace element contents of MIL generally support the conclusion that this dunite is a cumulate, not a mantle restite. The Yb and Sm contents of MIL are similar to those of diogenite MET 00422 (Barrat et al. 2008, 2010a), among the lowest determined for diogenites (Fig. 7c). MET 00436 has a lower Yb content, and Tatahouine a lower Sm content, whereas MET 00422 is lower in both elements. Most diogenites lie between fictive melts with CI Yb/Sm ratios and orthopyroxene adcumulates derived from such melts (calculated via mass balance; $D^{opx/L}{}_{Sm} = 0.0135$, $D^{opx/L}{}_{Yb} = 0.0872$, derived from Bédard 2007; using the 1310 °C melt compositions from Righter and Drake 1997). Thus, all diogenites but MET 00424 and Tatahouine can be explained as mixtures of cumulate orthopyroxene and trapped melt. MIL plots near the cumulate orthopyroxene line, but away from the MIL cumulate line (calculated assuming 95% olivine, 5% orthopyroxene; orthopyroxene/melt partition coefficients as above; $D^{oliv/L}{}_{Sm} = 0.0006$, $D^{oliv/L}{}_{Yb} = 0.0469$ from Beattie 1994) (Fig. 7c), implying that it must contain a trapped melt component. Less than 1% trapped melt mixed with the cumulus phases can explain the Sm and Yb budget of MIL.

The parent melt used in the example model for MIL has 5× CI Sm and Yb, and plots well within the field of possible diogenite parent melts in Fig. 7c (approximately 3–9× CI Sm and Yb). This field is calculated from mass balance by applying the orthopyroxene/melt partition coefficients given above to the Sm and Yb contents of those diogenites that plot on the "opx cumulate" line in Fig. 7c. Modeling cumulate chemistry has a high degree of uncertainty because small errors in partition coefficients translate into large effects in the calculated cumulate composition. Nevertheless, the trace element model is in concert with the argument made above that MIL represents a cumulate from the same or similar magma sequences that produced diogenites, and not a mantle restite.

The minor incompatible lithophile elements, Al and Ti, are in general agreement with the modeling of Sm and Yb. The concentration of these elements in MIL is low, and as was the case for Sm and Yb, the Al and Ti contents of MIL are close to diogenite MET 00422 (Fig. 7b). We have not attempted to model the Al and Ti contents partly because their olivine/melt partition coefficients are not well known. Another complicating factor is that chromite is a major host for Al and Ti in MIL (Table 1). MIL has a higher modal chromite content than is typical of diogenites as evidenced by its high bulk Cr content (Fig. 7a), and modeling an olivine-orthopyroxene-chromite cumulate is not possible for Al and Ti because their partitioning behavior in Cr-rich spinels is poorly known.

Mineral/melt partition coefficients for Co and Ni are higher for olivine than for orthopyroxene (e.g., Adam and Green 2006); consequently, the high Co content for MIL compared with diogenites is expected (Fig. 7d). We would expect that MIL would have a higher Ni content as well, but this is not the case. MIL has Ni content within the upper end of the range for diogenites. The moderately siderophile element contents of brecciated HEDs can be significantly affected by even small amounts of chondritic contamination (e.g., see Chou et al. 1976).

Figure 7d shows an example mixing line between an arbitrarily chosen low-Ni diogenite and a chondritic clast from the Ellemeet diogenite (Mittlefehldt 1994). The four-pointed star on the mixing line represents a 1% admixture of chondritic material to the low-Ni diogenite. As can be seen, the range in diogenite Ni contents could be entirely due to very small amounts of chondritic material. Small amounts of chondritic contamination do not affect the Co content as much as it affects the Ni content, and the range in Co contents observed for diogenites and MIL is innate to cumulate dunites, harzburgites, and orthopyroxenites on Vesta.

The case for Ni is more difficult to evaluate. Orthopyroxene separates show a range in Ni contents from <20 to 100 μg g^{-1} (Mittlefehldt 1994). The high Ni diogenite, LAP 03979, was described as an unbrecciated olivine diogenite (McBride et al. 2004). However, Beck and McSween (2010a) recognized that it contains two distinct lithologies; a more magnesian harzburgitic diogenite and a more ferroan diogenite. The high Ni content of LAP 03979 is not likely to be innate to the olivine-rich cumulate material, however. Olivine in this rock contains only 29 μg g^{-1} Ni (Shearer et al. 2010), which is lower than the whole-rock datum shown in Fig. 7d. We can only surmise that the analyzed sample may have contained more than the typical amount of metal, but we cannot establish this as fact. Two labeled diogenites, ALH 85015 and PCA 02008, are polymict, or possibly so. ALH 85015 has been considered a howardite (Berkley and Boynton 1992), although it was originally classified as a diogenite. The Antarctic Meteorite curator has recently re-evaluated its classification, and has concluded that its correct classification is as a diogenite because "…only one [thin section] shows eucritic material" (*Antarctic Meteorite Newsletter* vol. 33, number 1). This would indicate that ALH 85015 is a polymict diogenite, containing eucritic material formed by mixing on the surface of Vesta, increasing the probability that it may contain chondritic contamination. PCA 02008 is also a polymict diogenite and may be paired with three howardites based on their cosmogenic

nuclide contents (Welten et al. 2009). Again, this increases the likelihood that the high Ni content of this stone reflects chondritic contamination. The ranges shown for all, but the labeled diogenites plausibly represent true cumulate compositions.

Excluding the two polymict diogenites, MIL is within the high Ni end of the diogenite range. We have not observed chondritic clasts or eucritic material in the three thin sections we have examined, nor have Krawczynski et al. (2008), though small amounts of fine-grained chondritic or eucritic material in the matrix would be difficult to identify. There is no evidence that MIL is polymict, and we thus discount the possibility that its high Ni content is the result of chondritic contamination. As the Ni content of MIL is within the diogenite range, the parent melt for this olivine-rich cumulate must have had a lower Ni content than those for diogenites with the highest Ni. This is consistent with the inference from lithophile elements that the MIL parent magma was not more primitive than those of diogenites. The very high olivine content of MIL may simply represent a localized accumulation of olivine in an otherwise typical diogenitic intrusive body.

Melt Inclusions

The inclusions in MIL and diogenite olivine were probably melts that were trapped, and later crystallized into separate daughter phases, as is common for melt inclusions that cool relatively slowly in intrusive rocks (Roedder 1979; Bodnar and Student 2006). Multiple lines of evidence support this model.

Diffusive FeO-loss has been observed between melt inclusions and host olivines in many terrestrial rocks (e.g., Gurenko et al. 1992; Sobolev and Danyushevsky 1994). This FeO-loss leads to the crystallization of Mg-rich diopside from the trapped melt (Danyushevsky et al. 2000), and can lead to sulfide crystallization from parts of the melt incompatible with olivine (Danyushevsky et al. 2002). Also, inclusions that are trapped as melt may recrystallize to form very sharply faceted, negative-crystal forms (Roedder 1979, 1984). We observe Mg-rich diopside and abundant sulfide, indicative of FeO-loss, along with negative-crystal forms in the MIL olivine inclusions (Fig. 1), supporting the hypothesis that these inclusions were trapped as melts.

"Uniform phase ratio" is another criterion for distinguishing inclusions that were once melt from inclusions that were crystalline when incorporated into mineral hosts (Roedder 1984). Modal abundances of phases in MIL inclusions are relatively uniform, with the majority of inclusions containing approximately 40 vol% troilite, 30 vol% clinopyroxene, and 30 vol% chromite or metal. This uniform phase ratio was observed in ten inclusions across the three sections, nine of which were in section 17, and one in section 10. Deviations from this average are probably due to different slices through the inclusions, or are a result of different degrees of metastability (Roedder 1984).

The identification of similar melt inclusions in the olivine-rich achondrite QUE 93148 also supports our interpretation. Goodrich and Righter (2000) identified several types of inclusions in QUE 93148 olivine. Their "type 4" inclusions, which they concluded were trapped melt, have the same relative size, shape, and proportion of opaques to silicate as the inclusions in MIL. This supports the interpretation that the inclusions in MIL olivine were trapped as melt. It is important to note that Goodrich and Righter (2000) also identify olivine inclusions (types 1–3) that they hypothesize formed from exsolution of olivine. This hypothesis is primarily based on the symplectic and lamellar morphologies of the inclusions. We do not see any of these textures in MIL inclusions. If the inclusions in MIL did form through exsolution, symplectic and lamellar textures were probably erased during metamorphism, when the phases redistributed into a more equilibrated distribution (triple junctions).

Several processes can be invoked to explain the incorporation of melt inclusions in MIL olivine. First, melt may have been included during primary olivine growth. Second, melt may have infiltrated through cracks in the olivine and became trapped as melt inclusions as the cracks healed. This is supported by the linear distribution of inclusions in some grains (Fig. 9a), and similar occurrences in diogenite orthopyroxene (Gooley and Moore 1976). Also, some of the inclusions might have been formed when selvages of melt adhered to crystalline phases, which were both then included in olivine. A few of the MIL inclusions contain chromite with very high Cr#s (94), indicative of early crystallization from a melt (Bowman et al. 1999). It is possible that small, high Cr# chromite crystallized very early from the melt, adhered to small bits of melt, which were both then included in olivine. Finally, these inclusions may have been incorporated during "pseudo-secondary processes" (Roedder 1984), such as adcumulus growth. In such a scenario, olivine grains would have settled at the base or walls of the magma chamber and continued to grow outward at the expense of trapped intercumulus melt. As olivine expands, it incorporates portions of that trapped melt. The included melt would be trapped as inclusions near the edges of grains, where adcumulus growth occurred (Hunter 1996). The general distribution of inclusions away from the core of one of the larger grains may support this scenario (Fig. 9b).

We have presented sufficient evidence to conclude that these inclusions were trapped melts. Though it is

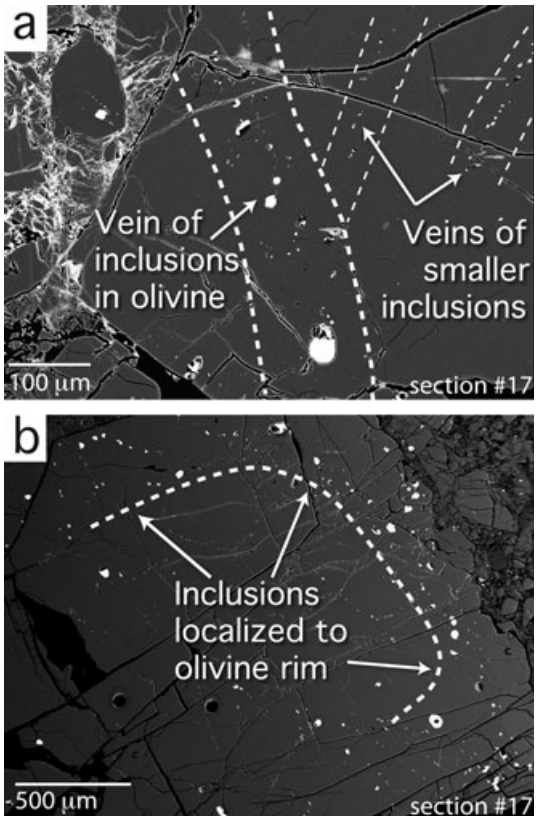

Fig. 9. Backscatter electron images showing the systematic distributions of melt inclusions in MIL 03443 olivine. a) Some inclusions display a linear distribution suggesting melt entry along fractures. b) Larger grains have inclusions concentrated near the rim, suggesting that melt was included during adcumulus growth.

possible that they exsolved from olivine, we think this is less likely.

CONCLUSIONS

1. Meteorite MIL 03443, a dunite breccia originally classified as a mesosiderite, is more likely a member of the HED group. Similarities in oxygen isotopes, silicate FeO/MnO ratios, and mineral compositions between MIL and the diogenites strongly support this grouping.
2. The observation of similar, unusual olivine inclusions in both MIL and the diogenites provides further evidence for their grouping. The uniform phase distribution, phases present, and general morphologies of these inclusions suggest that they were trapped as melt.
3. We present findings that suggest a cumulate origin for this meteorite. MIL contains more ferroan olivine and orthopyroxene relative to some diogenites. This, coupled with the presence of similar olivine inclusions in both groups, leads us to propose that MIL represents a cumulate akin to the diogenites, not a mantle restite.
4. Bulk compositional evidence supports a close link between MIL and diogenites as well. The trace element contents suggest a parent melt similar to those that produced diogenites. The olivine-rich nature of MIL plausibly reflects a localized accumulation of olivine in an otherwise typical diogenitic pluton.
5. As a cumulate that probably formed in one of the same plutons and by similar processes as diogenites, MIL should be classified as a dunitic diogenite.
6. Hubble Space Telescope and ground-based spectra were initially interpreted to show olivine-rich lithologies in the eastern hemisphere of Vesta (Binzel et al. 1997; Gaffey 1997). However, this conclusion has been challenged by subsequent studies (Li et al. 2010; Reddy et al. 2010). Similarly, ambiguity exists in the interpretation of HST spectra of the South Polar basin, which may show abundant olivine (Thomas et al. 1997). Our study provides evidence of an olivine-rich lithology in the HED suite, and thus supports the presence of such a lithology on Vesta.

Acknowledgments—The authors thank L. Fedele (Virginia Tech) and P. Luffi (Rice) for their assistance in this project, and A. Yamaguchi, K. Righter, and an anonymous reviewer for thoughtful reviews that significantly improved this manuscript. We also acknowledge C. Satterwhite for providing curation information, the MWG for allocating meteorite samples, and J. A. Barrat for his comments. This work was partially supported by NASA Cosmochemistry Grant NNG06GG36G to H. Y. M. Work done at JSC was funded by the NASA Cosmochemistry Program to D. W. M.

Editorial Handling—Dr. Akira Yamaguchi

REFERENCES

Abramoff M. D., Magelhaes P. J., and Ram S. J. 2004. Image processing with ImageJ. *Biophotonics International* 11:36–42.

Adam J. and Green T. 2006. Trace element partitioning between mica- and amphibole-bearing garnet lherzolite and hydrous basanitic melt: 1. Experimental results and the investigation of controls on partitioning behavior. *Contributions to Mineralogy and Petrology* 152:1–17.

Balta J. B. and Beck A. W. 2011. Magmatic cumulate textures preserved by trace elements in diogenite meteorites (abstract #1107). 41th Lunar and Planetary Science Conference. CD-ROM.

Barrat J. A., Gillet P., Lesourd M., Blichert-Toft J., and Poupeau G. R. 1999. The Tatahouine diogenite: Mineralogical and chemical effects of sixty-three years of terrestrial residence. *Meteoritics & Planetary Science* 34:91–97.

Barrat J. A., Beck P., Bohn M., Cotten J., Gillet P., Greenwood R. C., and Franchi I. A. 2006. Petrology and geochemistry of the fine-grained unbrecciated diogenite Northwest Africa 4215. *Meteoritics & Planetary Science* 41:1045–1057.

Barrat J. A., Yamaguchi A., Greenwood R. C., Benoit M., Cotton J., Bohn M., and Franchi I. 2008. Geochemistry of diogenites: Still more diversity in their parent melts. *Meteoritics & Planetary Science* 43:1759–1775.

Barrat J. A., Yamaguchi A., Zanda B., Bollinger C., and Bohn M. 2010a. Relative chronology of crust formation on asteroid Vesta: Insights from the geochemistry of diogenites. *Geochimica et Cosmochimica Acta* 74:6218–6231.

Barrat J. A., Greenwood R. C., Yamaguchi A., Bohn M., Bollinger C., and Franchi I. A. 2010b. Northwest Africa 2968/3329: Dunitic and diogenitic pebbles from the same mesosiderite fall? (abstract). *Meteoritics & Planetary Science* 45:A11.

Beattie P. 1994. Systematics and energetics of trace-element partitioning between olivine and silicate melts: Implications for the nature of mineral/melt partitioning. *Chemical Geology* 117:57–71.

Beck A. W. and McSween H. Y. 2010a. Diogenites as polymict breccias composed of orthopyroxenite and harzburgite. *Meteoritics & Planetary Science* 45:850–872.

Beck A. W. and McSween H. Y. 2010b. Connections between dunite MIL 03443 and the diogenite meteorites (abstract #1533). 40th Lunar and Planetary Science Conference. CD-ROM.

Bédard J. H. 2007. Trace element partitioning coefficients between silicate melts and orthopyroxene: Parameterizations of D variations. *Chemical Geology* 244:263–303.

Berkley J. L. and Boynton N. J. 1992. Minor/major element variation within and among diogenite and howardite orthopyroxenite groups. *Meteoritics* 27:387–394.

Binzel R. P., Gaffey M. J., Thomas P. C., Zellner B. H., Storrs A. D., and Wells E. N. 1997. Geologic mapping of Vesta from 1994 Hubble Space Telescope images. *Icarus* 128:95–103.

Bodnar R. J. and Student J. J. 2006. Melt inclusions in plutonic rocks: Petrography and microthermometry. In *Melt inclusions in plutonic rocks*, edited by Webster J. D. Montreal: Mineralogical Association of Canada. Short Course 36. pp. 1–26.

Bowman L. E., Spilde M. N., and Papike J. J. 1997. Automated energy dispersive spectrometer modal analysis applied to the diogenites. *Meteoritics & Planetary Science* 32:869–875.

Bowman L. E., Papike J. J., and Spilde M. N. 1999. Diogenites as asteroidal cumulates: Insights from spinel chemistry. *American Mineralogist* 84:1020–1026.

Bunch T. E., Wittke J. H., Rumble D. III., Irving A. J., and Reed B. 2006. Northwest Africa 2968: A dunite from 4 Vesta (abstract). *Meteoritics & Planetary Science* 41:A31.

Bunch T. E., Irving A. J., Wittke J. H., Kuehner S. M., Rumble D. III., and Sipiera P. P. 2010. Northwest Africa 5784, Northwest Africa 5968 and Northwest Africa 6157: More Vestan dunites and olivine diogenites (abstract). *Meteoritics & Planetary Science* 45:A27.

Chou C.-L., Boynton W. V., Bild R. W., Kimberlin J., and Wasson J. T. 1976. Trace element evidence regarding a chondritic component in howardite meteorites. Proceedings, 7th Lunar Science Conference. pp. 3501–3518.

Clayton R. N. and Mayeda T. K. 1996. Oxygen isotope studies of achondrites. *Geochimica et Cosmochimica Acta* 60:1999–2017.

Danyushevsky L. V., Della-Pasqua F. N., and Sokolov S. 2000. Re-equilibration of melt inclusions trapped by magnesian olivine phenocrysts from subduction-related magmas: Petrological implications. *Contributions to Mineralogy and Petrology* 138:68–83.

Danyushevsky L. V., McNeill A. W., and Sobolev A. V. 2002. Experimental and petrological studies of melt inclusions in phenocrysts from mantle-derived magmas: An overview of techniques, advantages and complications. *Chemical Geology* 183:5–24.

Delaney J. S., Prinz M., and Nehru C. E. 1980. Olivine clasts from mesosiderites and howardites—Clues to the nature of achondritic parent bodies. Proceedings, 11th Lunar and Planetary Science Conference. pp. 1073–1087.

Delaney J. S., Prinz M., and Takeda H. 1984. The polymict eucrites. Proceedings, 15th Lunar and Planetary Science Conference. *Journal of Geophysical Research* 89:C251–C288.

Desnoyers C. 1982. L'Olivine dans les howardites: Origine, et implications pour le corps parent de ces météorites achondritiques. *Geochimica et Cosmochimica Acta* 46:667–680.

Domanik K., Kolar S., Musselwhite D., and Drake M. J. 2004. Accessory silicate mineral assemblages in the Bilanga diogenite: A petrographic study. *Meteoritics & Planetary Science* 39:567–579.

Eales H. V. and Cawthorn R. G. 1996. The Bushveld Complex. In *Layered intrusions*, edited by Cawthorn R. G. Amsterdam: Elsevier Science. pp. 181–229.

Eggins S. M., Woodhead J. D., Kinsley L. P. J., Mortimer G. E., Sylvester P., McCulloch M. T., Hergt J. M., and Handler R. 1997. A simple method for precise determination of ≥40 trace elements in geological samples by ICPMS using enriched isotope internal standardisation. *Chemical Geology* 134:311–326.

Floran R. J., Prinz M., Hlava P. F., Keil K., Spettel B., and Wänke H. 1981. Mileralogy, petrology, and trace element geochemistry of the Johnstown meteorite: A brecciated orthopyroxenite with siderophile and REE-rich components. *Geochimica et Cosmochimica Acta* 45:2385–2391.

Fowler G. W., Papike J. J., Spilde M. N., and Shearer C. K. 1994. Diogenites as asteroidal cumulates: Insights from orthopyroxene major and minor element chemistry. *Geochimica et Cosmochimica Acta* 58:3921–3929.

Fowler G. W., Shearer C. K., Papike J. J., and Layne G. D. 1995. Diogenites as asteroidal cumulates: Insights from orthopyroxene trace element chemistry. *Geochimica et Cosmochimica Acta* 59:3071–3084.

Fredriksson K. and Keil K. 1963. The light-dark structure in the Pantar and Kapoeta stone meteorites. *Geochimica et Cosmochimica Acta* 27:717–739.

Fredriksson K., Noonan A., Brenner P., and Sudre C. 1976. Bulk and major phase composition of eight hypersthene achondrites (abstract). *Meteoritics* 11:278–280.

Fuhrman M. and Papike J. J. 1981. Howardites and ploymict eucrites: Regolith samples from the eucrite parent body.

Petrology of Bholgati, Bununu, Kapoeta, and ALHA76005. Proceedings, 12th Lunar and Planetary Science Conference. pp. 1257–1279.
Gaffey M. J. 1997. Surface lithologic heterogeneity of asteroid 4 Vesta. *Icarus* 127:130–157.
Goodrich C. A. 2002. Olivine-phyric martian basalts: A new type of shergottite. *Meteoritics & Planetary Science* 37:31–34.
Goodrich C. A. and Righter K. 2000. Petrology of unique achondrite Queen Alexandra Range 93148: A piece of the pallasite (howardite-eucrite-diogenite?) parent body? *Meteoritics & Planetary Science* 35:521–535.
Gooley R. and Moore C. B. 1976. Native metal in diogenite meteorites. *American Mineralogist* 61:373–378.
Govindaraju K. 1994. 1994 compilation of working values and sample descriptions for 383 geostandards. *Geostandards Newsletter* 18:1–158.
Greenwood R. C., Franchi I. A., Jambon A., and Buchanan P. C. 2005. Widespread magma oceans on asteroidal bodies in the early solar system. *Nature* 435:916–918.
Greenwood R. C., Franchi I. A., Jambon A., Barrat J. A., and Burbine T. H. 2006. Oxygen isotope variation in stony-iron meteorites. *Science* 313:1763–1765.
Guillong M., Horn I., and Gunther D. 2003. A comparison of 266 nm, 213 nm and 193 nm produced from a single solid state Nd:YAG laser for laser ablation. *Journal of Analytical Atomic Spectroscopy* 18:1224–1230.
Gurenko A. A., Sobolev A. V., and Kononkova N. N. 1992. New petrological data on Icelandic rift alkali basalts. *Geochemistry International* 29:41–53.
Herzberg C. T. and O'Hara M. J. 1985. Origin of mantle peridotite and komatiite by partial melting. *Geophysical Research Letters* 12:541–544.
Hewins R. H. 1981. Orthopyroxene-olivine assemblages in diogenites and mesosiderites. *Geochimica et Cosmochimica Acta* 45:123–126.
Hunter R. H. 1996. Texture development in cumulate rocks. In *Layered intrusions*, edited by Cawthorn R. G. Amsterdam: Elsevier Science. pp. 77–101.
Jackson E. D. 1961. Primary textures and mineral associations in the Ultramafic Zone of the Stillwater Complex. U. S. Geological Survey Professional Paper #358.
Kong P., Su W., Li X., Spettel B., Palme H., and Tao K. 2008. Geochemistry and origin of metal, olivine clasts, and matrix in the Dong Ujimqin Qi mesosiderite. *Meteoritics & Planetary Science* 43:451–460.
Krawczynski M. J., Elkins-Tanton L. T., and Grove T. L. 2008. Petrology of mesosiderite(?) MIL 03443,9; constraints on eucrite parent body bulk composition and magmatic processes (abstract #1229). 39th Lunar and Planetary Science Conference. CD-ROM.
Labotka T. C. and Papike J. J. 1980. Howardites: Samples of the regolith of the eucrite parent-body. Petrology of Frankfort, Pavlovka, Yurtuk, Malvern, and ALHA77302. Proceedings, 11th Lunar and Planetary Science Conference. pp. 1103–1130.
Li J.-Y., McFadden L. A., Thomas P. C., Mutchler M. J., Parker J. W., Young E. F., Russell C. T., Sykes M. V., and Schmidt B. E. 2010. Photometric mapping of asteroid 4 Vesta's southern hemisphere with Hubble Space Telescope. *Icarus* 208:238–251.
Lorenz C. A., Nazarov M. A., Branstaetter F., and Ntaflos T. 2010. Metasomatic alteration of olivine inclusions in the Budulan mesosiderite. *Petrology* 18:461–470.
Mayne R. G., McSween H. Y., McCoy T. J., and Gale A. 2009. Petrology of the unbrecciated eucrites. *Geochimica et Cosmochimica Acta* 73:794–819.
McBride K. and McCoy T. J. 2006. *Antarctic Meteorite Newsletter* 29:32.
McBride K., McCoy T. J., and Welzenbach L. 2004. *Antarctic Meteorite Newsletter* 27:19.
McCall G. J. and Cleverly W. H. 1965. Newly discovered mesosiderite containing achondrite fragments; the Mount Padbury mesosiderite. *Nature* 207:851.
McCarthy T. S., Ahrens L. H., and Erlank A. J. 1972. Further evidence in support of the mixing model for howardite origin. *Earth and Planetary Science Letters* 15:86–93.
McSween H. Y, Mittlefehldt D. W., Beck A. W., Mayne R. G., and McCoy T. J. 2011. HED meteorites and their relationship to the geology of Vesta and the Dawn mission. *Space Science Reviews*, doi:10.1007/s11214-010-9637-z.
Mittlefehldt D. W. 1979. Petrographic and chemical characterization of igneous lithic clasts from mesosiderites and howardites and comparison with eucrites and diogenites. *Geochimica et Cosmochimica Acta* 43:1917–1935.
Mittlefehldt D. W. 1980. The composition of mesosiderite olivine clasts and implications for the origin of pallasites. *Earth and Planetary Science Letters* 51:29–40.
Mittlefehldt D. W. 1994. The genesis of diogenites and HED parent body petrogenesis. *Geochimica et Cosmochimica Acta* 58:1537–1552.
Mittlefehldt D. W. 2000. Petrology and geochemistry of the Elephant Moraine A79002 diogenite. *Meteoritics & Planetary Science* 35:901–912.
Mittlefehldt D. W. 2002. Geochemistry of new, unusual diogenites and constraints on diogenite genesis (abstract). *Meteoritics & Planetary Science* 37:A100.
Mittlefehldt D. W. 2008. Meteorite dunite breccia MIL 03443: A probable crustal cumulate closely related to diogenites from the HED parent asteroid (abstract #1919). 39th Lunar and Planetary Science Conference. CD-ROM.
Mittlefehldt D. W. and Lindstrom M. M. 1993. Geochemistry and petrology of a suite of ten Yamato HED meteorites. *Antarctic Meteorite Research* 6:268.
Mittlefehldt D. W. and Lindstrom M. M. 2003. Geochemistry of eucrites: Genesis of basaltic eucrites, and Hf and Ta as petrogenetic indicators for altered antarctic eucrites. *Geochimica et Cosmochimica Acta* 67:1911–1935.
Mittlefehldt D. W., Chou C.-L., and Wasson J. T. 1979. Mesosiderites and howardites; igneous formation and possible genetic relationships. *Geochimica et Cosmochimica Acta* 43:673–688.
Mittlefehldt D. W., McCoy T. J., Goodrich C. A., and Kracher A. 1998. Non-chondritic meteorites from asteroidal bodies. In *Planetary materials*, edited by Papike J. J. Reviews in Mineralogy and Geochemistry, vol. 36. Washington, D.C.: Mineralogical Society of America. pp. 4.1–4.195.
Mittlefehldt D. W., Beck A. W., Lee C-T. A., McSween H. Y., Buchanan P. C., and Burbine T. Forthcoming. Compositional constraints on the genesis of diogenites. *Meteoritics & Planetary Science*.
Mutchler S. T., Fedele L., and Bodnar R. J. 2008. Analysis Management System (AMS) for reduction of laser ablation ICP-MS data. In *Laser ablation ICP-MS in the earth sciences: Current practices and outstanding issues*, edited by Sylvester P. Montreal: Mineralogical Association of Canada. Short Course 40. pp. 503–353.

Nehru C. E., Zucker S. M., Harlow G. E., and Prinz M. 1980. Olivines and olivine coronas in mesosiderites. *Geochimica et Cosmochimica Acta* 44:1103–1118.

Ntaflos T., Kurat G., Koeberl C., and Brandstatter F. 1993. Mincy dunite F6241B: The missing ultramafic component from mesosiderites (abstract). *Meteoritics* 28:414.

Pallister J. S. and Hopson C. A. 1981. Samail ophiolite plutonic suite: Field relations, phase variation, cryptic variation and layering, and a model of a spreading ridge magma chamber. *Journal of Geophysical Research* 86:2593–2644.

Papike J. J. 1981. Silicate mineralogy of planetary basalts. In *Basaltic volcanism on the terrestrial planets*, edited by Merrill R. B. and Ridings R. New York: Pergamon. pp. 340–363.

Papike J. J., Karner J. M., and Shearer C. K. 2001. Mn-Fe systematics in pyroxene from planetary basalts: An indicator of planetary parentage (abstract). 32nd Lunar and Planetary Science Conference. p. 1009.

Papike J. J., Karner J. M., and Shearer C. K. 2003. Determination of planetary basalt parentage: A simple technique using the electron microprobe. *American Mineralogist* 88:469–472.

Papike J. J., Karner J. M., and Shearer C. K. 2004. Comparative planetary mineralogy: V/(Cr + Al) systematics in chromite as an indicator of relative oxygen fugacity. *American Mineralogist* 89:1557–1560.

Powell B. N. 1971. Petrology and chemistry of mesosiderites—II. Silicate textures and compositions and metal-silicate relationships. *Geochimica et Cosmochimica Acta* 35:11–34.

Prinz M., Delaney J. S., Harlow G. E., Bedell R. L., and Nehru C. E. 1980. Modal studies of mesosiderites and related achondrites, including the new mesosiderite ALHA77219. Proceedings, Lunar and Planetary Science Conference. pp. 1055–1071.

Reddy V., Gaffey M. J., Kelley M. S., Nathues A., Li J.-Y., and Yarbrough R. 2010. Compositional heterogeneity of Asteroid 4 Vesta's southern hemisphere: Implications for the Dawn mission. *Icarus* 210:693–706.

Righter K. and Drake M. J. 1997. A magma ocean on Vesta: Core formation and petrogenesis of eucrites and diogenites. *Meteoritics & Planetary Science* 32:929–944.

Roedder E. 1979. Origin and significance of magmatic inclusions. *Bulletin de Mineralogie* 102:487–510.

Roedder E. 1984. *Fluid inclusions*. Reviews in Mineralogy and Geochemistry, vol. 12. Washington, D.C.: Mineralogical Society of America.

Rubin A. E. 1997. Mineralogy of meteorite groups. *Meteoritics & Planetary Science* 32:231–247.

Rumble D. III. and Hoering T. C. 1994. Analysis of oxygen and sulfur isotopes ratios in oxide and sulfide minerals by spot heating with a carbon dioxide laser in a fluorine atmosphere. *Accounts of Chemical Research* 27:237–241.

Rumble D. III., Farquhar J., Young E. D., and Christensen C. P. 1997. In situ oxygen isotope analysis with an excimer laser using F_2 and BrF_5 reagents and O_2 gas as analyte. *Geochimica et Cosmochimica Acta* 61:4229–4234.

Rumble D. III., Miller M. F., Franchi I. A., and Greenwood R. C. 2007. Oxygen three-isotope fractionation lines in terrestrial silicate minerals: An inter-laboratory comparison of hydrothermal quartz and eclogitic garnet. *Geochimica et Cosmochimica Acta* 71:3592–3600.

Ruzicka A., Boynton W. V., and Ganguly J. 1994. Olivine coronas, metamorphism, and the thermal history of the Morristown and Emery mesosiderites. *Geochimica et Cosmochimica Acta* 58:2725–2741.

Ruzicka A., Snyder G. A., and Taylor L. A. 1997. Vesta as the howardite, eucrite and diogenite parent body: Implications for the size of a core and for large-scale differentiation. *Meteoritics & Planetary Science* 32:825–840.

Sack R. O., Azeredo W. J., and Lipschutz M. E. 1991. Olivine diogenites: The mantle of the eucrite parent body. *Geochimica et Cosmochimica Acta* 55:1111–1120.

Scott E. R. D., Greenwood R. C., Franchi I. A., and Sanders I. S. 2009a. Oxygen isotopic constraints on the origin and parent bodies of eucrites, diogenites, and howardites (abstract #2263). 40th Lunar and Planetary Science Conference. CD-ROM.

Scott E. R. D., Greenwood R. C., Franchi I. A., and Sanders I. S. 2009b. Oxygen isotopic constraints on the origin and parent bodies of eucrites, diogenites, and howardites. *Geochimica et Cosmochimica Acta* 73:5835–5853.

Sharp Z. D. 1990. A laser-based microanalytical method for the in-situ determination of oxygen isotope ratios of silicates and oxides. *Geochimica et Cosmochimica Acta* 54:1353–1357.

Shearer C. K., Burger P., and Papike J. J. 2010. Petrogenetic relationships between diogenites and olivine diogenites: Implications for magmatism on the HED parent body. *Geochimica et Cosmochimica Acta* 74:4865–4880.

Shestopalov D. I., McFadden L. A., Golubeva L. F., and Orujova L. O. 2010. About mineral composition of geologic units in the northern hemisphere of Vesta. *Icarus* 209:575–585.

Sobolev A. V. and Danyushevsky L. V. 1994. Petrology and geochemistry of boninites from the north termination of the Tonga Trench—Constraints on the generation conditions of primary high-Ca boninite magmas. *Journal of Petrology* 35:1183–1211.

Stolper E. 1977. Experimental petrology of eucritic meteorites. *Geochimica et Cosmochimica Acta* 41:587–611.

Sylvester P. 2008. Chapter 5. Matrix effects in laser ablation ICPMS. In *Laser ablation ICP-MS in the earth sciences: Current practices and outstanding issues*, edited by Sylvester P. Montreal: Mineralogical Association of Canada. Short Course 40: pp. 67–78.

Takeda H. 1997. Mineralogical records of early planetary processes on the howardite, eucrite, diogenite parent body with reference to Vesta. *Meteoritics & Planetary Science* 32:841–853.

Tamura A. and Arai S. 2006. Harzburgite-dunite-orthopyroxenite suite as a record of supra-subduction zone setting for the Oman ophiolite mantle. *Lithos* 90:43–56.

Thomas P. C., Binzel R. P., Gaffey M. J., Storrs A. D., Wells E. N., and Zellner B. H. 1997. Impact excavation asteroid 4 Vesta: Hubble Space Telescope results. *Science* 227:1492–1495.

Valley J. W., Kitchen N. E., Kohn M. J., Niendorf C. R., and Spicuzza M. J. 1995. UWG-2, a garnet standard for oxygen isotope ratios: Strategies for high precision and accuracy with laser heating. *Geochimica et Cosmochimica Acta* 59:5223–5231.

Wadhwa M., Shukolyukov A., Davis A. M., Lugmair G. W., and Mittlefehldt D. W. 2003. Differentiation history of the mesosiderite parent body: Constraints from trace elements and manganese-chromium isotope systematics in Vaca Muerta silicate clasts. *Geochimica et Cosmochimica Acta* 67:5047–5069.

Warren P. H., Kallemeyn G. W., Huber H., Ulff-Møller F., and Choe W. 2009. Siderophile and other geochemical constraints on mixing relationships among HED-meteoritic breccias. *Geochimica et Cosmochimica Acta* 73:5918–5943.

Welten K. C., Caffee M. W., and Beck A. W. 2009. Cosmogenic radionuclides in three paired howardites and a polymict diogenite from Pecora Escarpment icefield, Antarctica (abstract). *Meteoritics & Planetary Science* 44:A216.

Wiechert U. H., Halliday A. N., Palme H., and Rumble D. 2004. Oxygen isotope evidence for rapid mixing of the HED meteorite parent body. *Earth and Planetary Science Letters* 221:373–382.